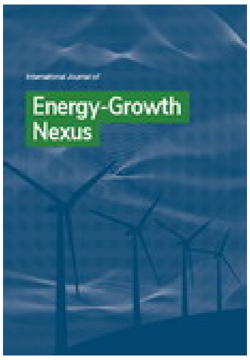

International Journal of the Energy-Growth Nexus

ISSN online: 2753-7617 - ISSN print: 2753-7609
https://www.inderscience.com/ijegn

Advanced Heffron-Phillips model for improving power system stability

Niharika Agrawal, Faheem Ahmed Khan, Mamatha Gowda

DOI: 10.1504/IJEGN.2023.10059201

Article History:

Received:	09 February 2023
Last revised:	10 February 2023
Accepted:	14 June 2023
Published online:	04 December 2023

Advanced Heffron-Phillips model for improving power system stability

Niharika Agrawal* and Faheem Ahmed Khan

Department of Electrical and Electronics Engineering,
Ghousia College of Engineering,
Ramanagaram District – 562159, Karnataka, India
Email: niharika.svits@gmail.com
Email: faheemahmedkhan11@gmail.com
*Corresponding author

Mamatha Gowda

Department of Artificial Intelligence and Data Science,
BGS College of Engineering and Technology,
Mahalakshmi Puram, Bengaluru,
560086, Karnataka, India
Email: mahesh.mamatha@gmail.com

Abstract: The smooth working of the power system is essential for the economic and technological development of the country. But the power system experience low-frequency oscillations (LFOs) due to various disturbances. These LFOs if not controlled, grow and cause the system to collapse. The stability of the system has been analysed with Heffron-Phillips model based on six K-constants with the synchronous generator (SG) model no. 1.0. In the present work, a higher-order SG model 1.1 is used for designing a novel and improved model for damping oscillations in the system and is called an advanced Heffron-Phillips model (AHPM). Three different cases and algorithms are considered. It is concluded that the system is stable, safe, and secure with PSS based on snake optimisation technique. The optimisation and artificial intelligence techniques produced excellent damping results. This model is also capable of meeting the challenges of grid integration with renewables.

Keywords: damping; eigenvalues; EVS; optimisation; oscillations; performance; power system.

Reference to this paper should be made as follows: Agrawal, N., Khan, F.A. and Gowda, M. (2023) 'Advanced Heffron-Phillips model for improving power system stability', *Int. J. Energy-Growth Nexus*, Vol. 1, No. 1, pp.63–89.

Biographical notes: Niharika Agrawal received her BE and ME in Electrical Engineering from the SGSITS Engineering College, Madhya Pradesh, Indore. She has worked as an Assistant Professor in the Electrical and Electronics Engineering Department in Madhya Pradesh and Bangalore. Currently, she is working towards her PhD at the Ghousia College of Engineering, Ramanagaram, Karnataka from VTU. Her research interest includes power system, renewable energy, microgrids, soft computing, control systems, and power quality.

Faheem Ahmed Khan is a Professor and the Director of Research and Development in the Department of EEE, Ghousia College of Engineering, Ramanagaram in Karnataka State of India. He obtained his Bachelor of Engineering from the SJCE Mysore and Master's degree from the UVCE, Bengaluru and completed his PhD from the JNTU Hyderabad in the field of High Voltage Engineering. He has presented over 50 papers in national and international journals including IEEE-TDEI. His research area includes high voltage engineering, power system engineering and control engineering. He has 25 years of teaching and two years of Industrial experience. He has been awarded with 'Award for Research Publications' from Vision Group on Science and Technology (VGST), Karnataka.

Mamatha Gowda has received her Bachelor degree from the Mangalore University, Master's degree from the Bangalore and Doctorate from the Prairie View A&M University, Texas, USA in the field of Electrical Engineering. She has 17 years of teaching experience and five years of industrial experience. Her areas of research interest are power electronics, motor drives and controls, renewable energy, power systems and control systems. Currently, she is serving as a Professor and the Head in AI and DS Department at BGS College of Engineering and Technology, Bangalore.

1 Introduction

The synchronous generator (SG) dynamics is based on Park's voltage equations. The coordinate system consists of d- and q-axis with a field winding 'f' on the direct (d)-axis. The dynamics of the single machine infinite bus system (SMIBS) is studied using the Heffron-Phillips model based on six K-constants. This model is based on SG model no. 1.0 which is the third order model. SG model no 1.1 is a fourth-order model and is called a two-axis model in references. This model includes the field winding dynamics on the d-axis and one damper winding dynamics on the q-axis. This is a detailed model and it is used in the present paper for the design of a novel advanced Heffron-Phillips model (AHPM) of SMIBS for stability studies. This AHPM is based on ten K-constants to represent the dynamics of the system instead of six K-constants in the old Heffron-Phillips model (OHPM). This SG model 1.1 is a better model as the dynamics of exciter can be easily incorporated here, it is a detailed model, the dynamics of d-axis internal voltage are not neglected here and it gives a better damping analysis of the system. In this paper the small signal stability (SSS) analysis of SMIBS is done using AHPM (Padhy and Panda, 2021; Sahu et al., 2021).

For studying the stability of OHPM the system's linearisation is essential with the consideration of a small disturbance. The disturbances create low-frequency oscillations (LFOs) in the system whose frequency range is from 0.1 to a few Hz. These oscillations if not controlled will grow and cause the system separation. These oscillations are manifested in the form of movement of the generator's angular position in the system. Between the 1970s and 1980s, the LFOs were manifested in the power transmission system from Scotland to England in Great Britain. It was due to the heavy loading of lines. In 1984 the oscillations were observed in the Taiwan network when a big amount of power was transferred on some high-voltage line. In 1996 there was an outage of the WSCC network which created power oscillations. The prime cause of these oscillations is the negative/poor damping of the electromechanical oscillation modes of the system. After a disturbance, there is a change in the electromagnetic torque of SG. This torque can be resolved into two components the synchronising (T_S) and damping torque (T_d) components. The lack of these torques lead to non-oscillatory instability and LFOs respectively. Automatic voltage regulator with high gain and fast action provided the necessary (T_S) but not the required (T_d). The AVRs were added to eliminate the voltage variations at the terminals of the generator. But fast-acting AVRs produced negative damping to the oscillations hence the need for a supplementary damping controller PSS was identified. The PSS was introduced in the system with AVR to provide the necessary. The role of PSS was to dampen out these LFOs and to improve the system stability. The conventional PSS was designed based on fixed parameters and hence was not suitable for changing operating conditions. The PSS was designed using pole placement, pole assignment, variable structure control, etc. For dealing with the problem of changing operating conditions the PSS was designed then using optimisation techniques and neural networks. These PSS were designed using various algorithms like genetic algorithm, particle swarm optimisation, artificial bee colony, ant colony, Harris Hawk, cuckoo search, etc. (Panda, 2009; Mahapatra et al., 2019, 2020).

In the present paper, the parameters of PSS are tuned using a novel meta-heuristic snake optimisation algorithm (SOA) having the key benefits of exploration and exploitation for SMIBS. This SOA has been tested on various functions like Zakharov, Rosenbrock and Rastrigin's cigar, hybrid, and composition functions. The different statistical results the average, mean, median, and standard deviation has been compared with other algorithms and they are found to be better with SOA. The SOA maintains a perfect balance between exploration and exploitation which is important and essential for any algorithm. Despite the promising results of other algorithms, SOA is implemented for tuning the parameters of PSS. This is due to the belief of the no free lunch (NFL) theory which mentions that there is always a scope for improvement and learning. NFL theory mentions that it is not possible for any optimisation algorithm to solve all the problems.

In order to validate and analyse the different algorithms and technologies the following three cases are discussed here.

Case a Damping performance comparison with GOA, MFOA and SOA algorithms with AHPM.

Case b Damping performance comparison between the traditional PID and PSS both based on SOA with AHPM.

Case c Damping performance comparison between the traditional PID and artificial neural network (ANN)-based controller with AHPM.

The novel contributions of the paper are:

1 Implementation of higher order SG model 1.1.

2 Five state variables in state matrix instead of earlier 4.

3 Considering the dynamics of internal voltage along d-axis.

4 The use of fourth order model instead of earlier third order model.

5 Using recent algorithm SOA proposed in knowledge-based system.

6 The eigenvalue analysis of the system with GOA, MFOA and SOA.

7 The participation factor analysis of the system with three algorithms.

8 The time domain simulation analysis of the system and comparison of three algorithms.

9 The design of PID controller with AHPM.

10 The comparison between PID and PSS both based on SOA.

11 The comparison between PID and ANN-based controller.

2 Materials and methods

2.1 SG modelling

Synchronous machines (SM) are the most important element of the power system. These machines are represented by the d and q-axis park model. The SM has three-phase armature windings on the stator which are the 'a' winding, the 'b' winding and the 'c' winding. There are four windings on the rotor which are 'f', 'h', 'g', and 'k'. The field winding is 'f'. The 'h', 'g', and 'k' are the damper coils. The traditional, or OHPM, is based on SG model 1.0, which is a third-order model known as a one-axis flux decay model and has six K-constants. In the present paper, a higher-order SG model 1.1, a fourth-order model, is used for the development of the Heffron-Phillips model for stability analysis, and it is called an AHPM. In the present paper, the fourth-order model is used for the design of a novel AHPM instead of the third-order model in OHPM and is based on the following equations (Jyothi et al., 2021; Das et al., 2022).

2.2 Old Heffron-Phillips model

A single machine connected to infinite bus with a transmission line shown in Figure 2. It is checked for the stability analysis under small disturbances/perturbations with SOA in this paper. The mathematical analysis of the model is based on system equations and six K-constants which are derived after linearising the system around an operating point. The derivation of these six constants was done firstly by Heffron and Phillips and hence this model is popular as Heffron-Phillips model (Nie et al., 2019). The transfer function model of OHPM with six K-constants is given in Figure 1.

$$K_1 = \frac{\partial P_t}{\partial \delta}, K_2 = \frac{\partial P_t}{\partial E_q'}, K_3 = \frac{\partial E_q}{\partial E_q'}, K_4 = \frac{\partial E_q}{\partial \delta}, K_5 = \frac{\partial V_t}{\partial \delta}, K_6 = \frac{\partial V_t}{\partial E_q'}$$

2.3 The AHPM

For including the dynamics of internal voltage along d-axis there is one more state variable in state matrix. In OHPM the state vector X is $[\Delta\delta\ \Delta\omega\ \Delta E_q'\ \Delta E_{fd}']^T$. In AHPM the state vector X is $[\Delta\delta\ \Delta\omega\ \Delta E_q'\ \Delta E_d'\ \Delta E_{fd}']^T$. The system equations including ten K-constants are:

$$\Delta\dot{\delta} = \omega_b \Delta\omega_m \tag{1}$$

$$\Delta\dot{\omega}_m = -\frac{D}{2H}\Delta\omega_m + \frac{1}{2H}\Delta T_m - \frac{K_1}{2H}\Delta\delta - \frac{K_2}{2H}\Delta E_q' - \frac{K_3}{2H}\Delta E_d' \tag{2}$$

$$\Delta\dot{E}_q' = \frac{1}{T_{d0}'}\left(\Delta E_{fd} - K_5\Delta\delta - \frac{\Delta E_q'}{K_4}\right) \tag{3}$$

$$\Delta\dot{E}_d' = \frac{1}{T_{q0}'}\left(K_7\Delta\delta - \frac{\Delta E_d'}{K_6}\right) \tag{4}$$

$$\Delta\dot{E}_{fd} = -\frac{K_A K_8}{T_A}\Delta\delta - \frac{K_A K_9}{T_A}\Delta E_q' - \frac{K_A K_{10}}{T_A}\Delta E_d' + \frac{K_A}{T_A}\Delta V_{ref} - \frac{1}{T_A}\Delta E_{fd} \tag{5}$$

Figure 1 The OHPM (see online version for colours)

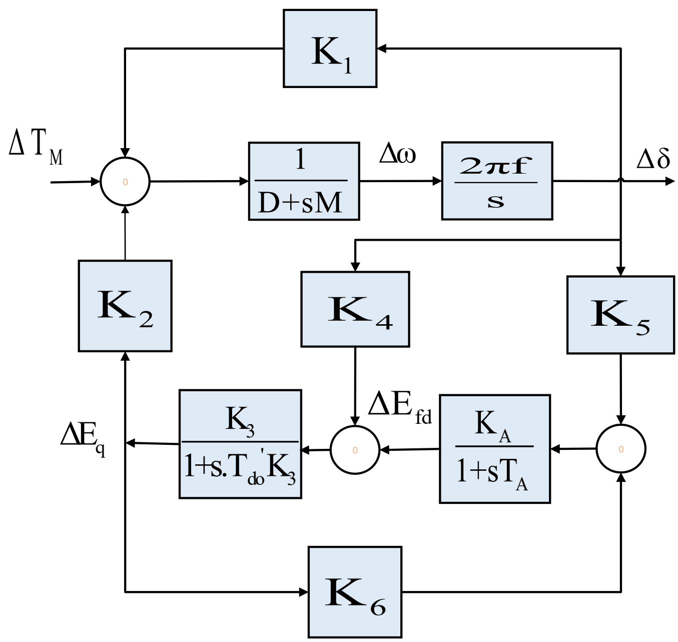

2.4 The SMIBS with PSS and exciter

The PSS is added in SMIBS to mitigate the problem of oscillations created due to negative torque produced by AVR. An additional voltage stabilising signal (V_S) is added as an input signal to the system. This signal is generated by PSS whose input is rotor speed deviation (ω). The different input signals to the PSS can be frequency, rotor speed, electrical power, or some combination of these signals. Figure 2 shows the diagram of the SMIBS with PSS included. G stands for SG.

Figure 4 shows the PSS lead lag structure (PSSLLS). The PSSLLS has a gain block with constant, washout block (WOB) which acts as a high-pass filter and two stage lead-lag compensator block to compensate for the phase lag between the output and input signals. When the operating conditions change the conventional PSSLLS may or may not produce the adequate/required damping for SMIBS hence alternatives or algorithms are needed to add in OHPM (Anantwar et al., 2019; Mallikarjunaswamy et al., 2020).

Figure 2 The novel AHPM (see online version for colours)

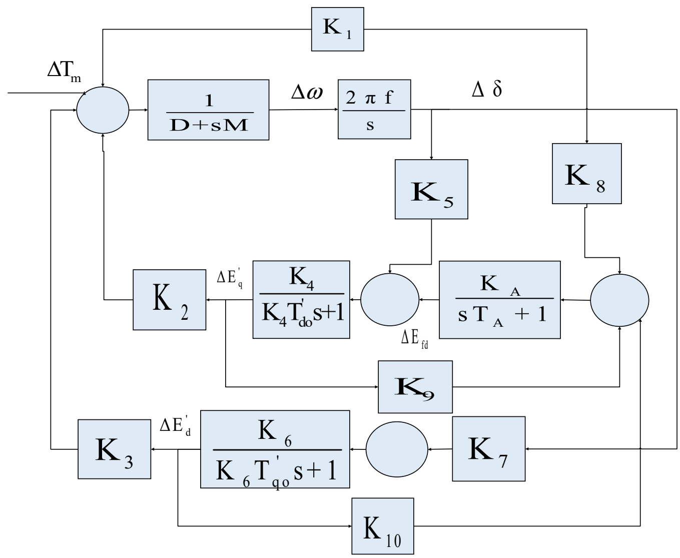

Figure 3 SMIBS with PSS (see online version for colours)

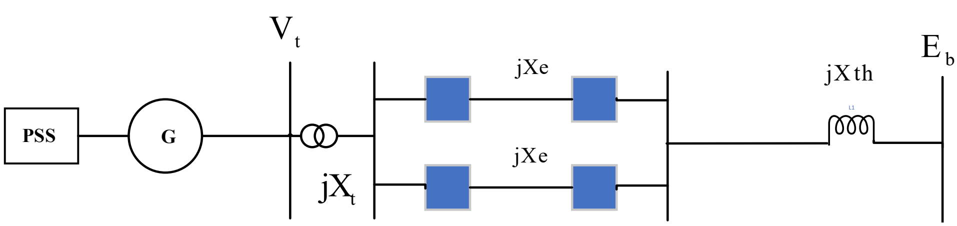

Figure 4 The PSS lead-lag structure (see online version for colours)

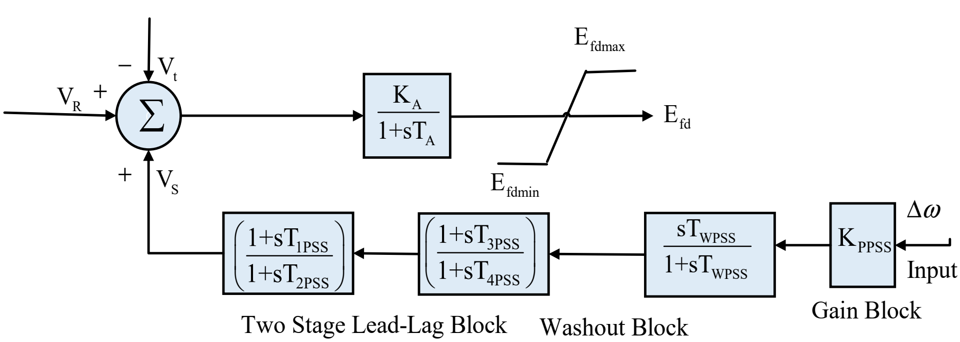

2.5 State space representation of the SMIBS with model 1.1

There are now five state variables instead of four state space variables in old HP model. The equations involving the state space model are: $\dot{X} = AX + BU$ and Y = CX + DU, where A, B, C, D are the constant matrices and X, Y, U are the state, input and output vectors (Gandhi and Joshi, 2013). Figure 5 shows the AHPM with PSS.

Figure 5 The AHPM with PSS (see online version for colours)

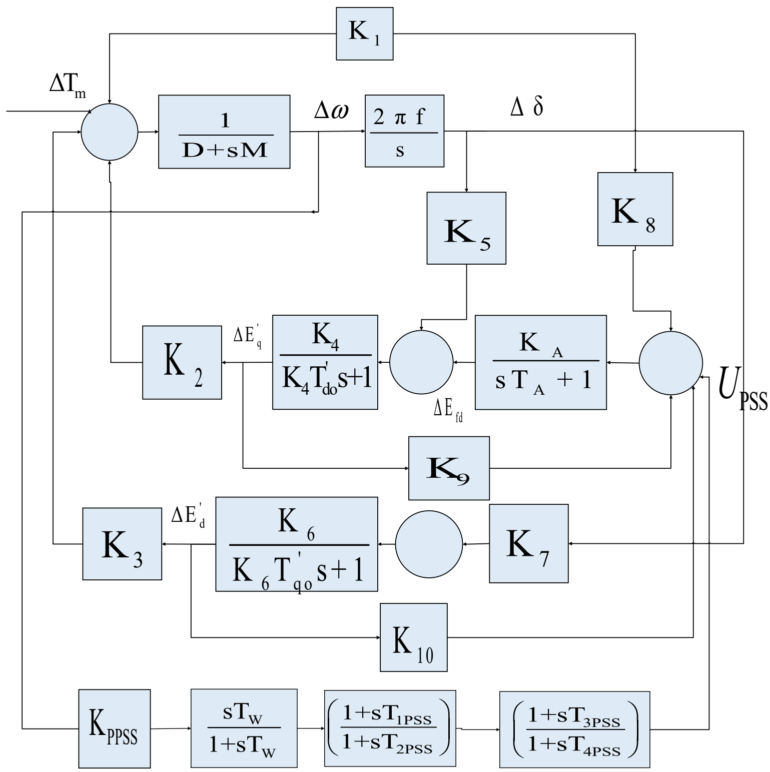

2.6 Development of state matrix A based on PSS parameters

The various equations involving the development of A matrix are (Gandhi and Joshi, 2019):

$$\Delta\dot{E}_{fd} = -\frac{K_A K_8}{T_A}\Delta\delta - \frac{K_A K_9}{T_A}\Delta E'_q - \frac{K_A K_{10}}{T_A}\Delta E'_d + \frac{K_A}{T_A}\Delta V_{ref} - \frac{1}{T_A}\Delta E_{fd} + \frac{K_A}{T_A}V_{PSS} \quad (6)$$

$$\dot{E}_{FD} = \frac{1}{T_A}E_{FD} + \frac{K_A}{T_A}\left(V_{ref} - V_t + V_{PSS}\right) \quad (7)$$

Figure 6 The PSS with three more state variables (see online version for colours)

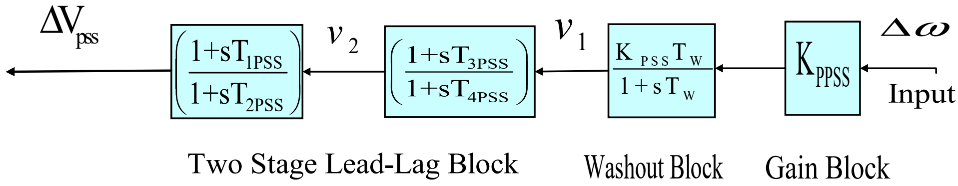

There are now three more state variables given in equations:

$$\Delta\dot{v}_1 = -\frac{K_1 K_{PSS}}{2H}\Delta\delta - \frac{DK_{PSS}}{2H}\Delta\omega_m - \frac{K_2 K_{PSS}}{2H}\Delta E_q' - \frac{K_3 K_{PSS}}{2H}\Delta E_d' - \frac{1}{T_W}\Delta v_1 \tag{8}$$

$$\Delta\dot{v}_2 = -a_1\Delta\delta - a_2\Delta\omega_m - a_3\Delta E_q' - a_4\Delta E_d' - a_5\Delta v_1 + a_6 v_2 \tag{9}$$

$$\Delta\dot{v}_{pss} = -b_1\Delta\delta - b_2\Delta\omega_m - b_3\Delta E_q' - b_4\Delta E_d' + b_5\Delta v_1 + b_6 v_2 + b_7 v_{pss} \tag{10}$$

The A matrix based on above equations is

$$\begin{bmatrix}
0 & \omega_B & 0 & 0 & 0 & 0 & 0 & 0 \\
-\frac{K_1}{2H} & -\frac{D}{2H} & -\frac{K_2}{2H} & -\frac{K_3}{2H} & 0 & 0 & 0 & 0 \\
\frac{-K_5}{T_{d0}'} & 0 & -\frac{1}{T_{d0}' K_4} & 0 & \frac{1}{T_{d0}'} & 0 & 0 & 0 \\
\frac{K_7}{T_{q0}'} & 0 & 0 & -\frac{1}{T_{q0}' K_6} & 0 & 0 & 0 & 0 \\
-\frac{K_A K_8}{T_A} & 0 & -\frac{K_A K_9}{T_A} & -\frac{K_A K_{10}}{T_A} & -\frac{1}{T_A} & 0 & 0 & \frac{K_A}{T_A} \\
-\frac{K_1 K_{PSS}}{2H} & -\frac{DK_{PSS}}{2H} & -\frac{K_2 K_{PSS}}{2H} & -\frac{K_3 K_{PSS}}{2H} & 0 & -\frac{1}{T_W} & 0 & 0 \\
a_{71} & a_{72} & a_{73} & a_{74} & a_{75} & a_{76} & a_{77} & a_{78} \\
a_{81} & a_{82} & a_{83} & a_{84} & a_{85} & a_{86} & a_{87} & a_{88}
\end{bmatrix}$$

Here the values of elements of a are based on time constant parameters of PSS and machine parameters. Here the state vector is

$$\dot{X} = \left[\Delta\dot{\delta} \quad \Delta\dot{\omega}_m \quad \Delta\dot{E}_q' \quad \Delta\dot{E}_q' \quad \Delta\dot{E}_{fd}' \quad \Delta\dot{v}_1' \quad \Delta\dot{v}_2' \quad \Delta\dot{V}_{PSS}\right]^T.$$

The detailed explanation of the terms is explained in Padiyar (2008).

2.7 *Schematic block diagram with three algorithms*

The different types of PSS are shown in Figure 7. The parameters of PSS are tuned using three different algorithms which are the genetic optimisation algorithm (GOA), the moth-flame optimisation algorithm (MFOA), and the novel SOA (Hesham et al., 2021).

Figure 7 The schematic block diagram (see online version for colours)

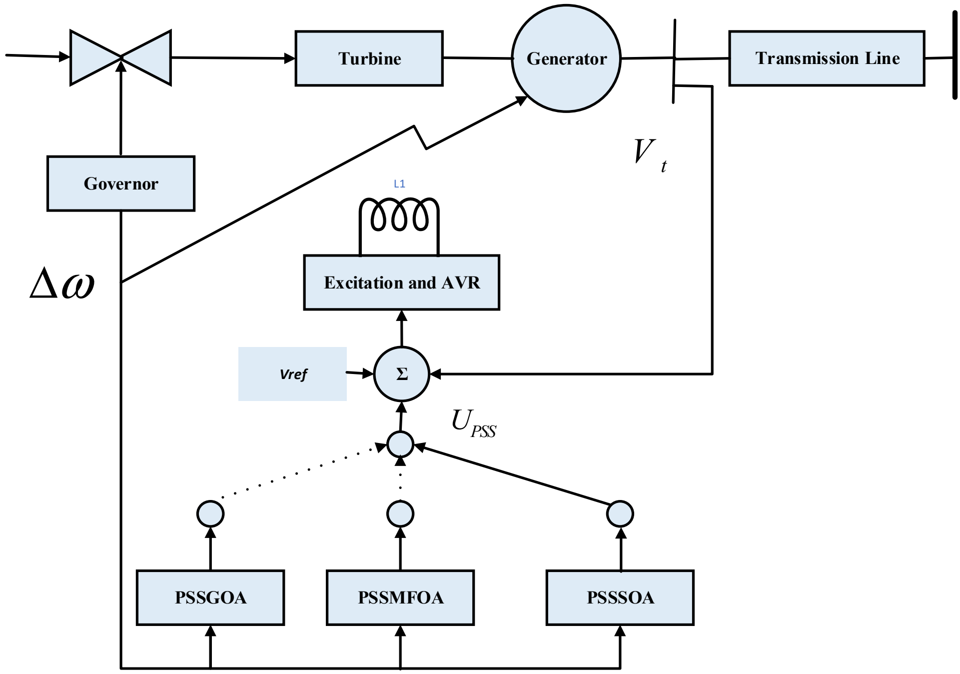

2.8 Development of AHPM with PID controller

Different controllers are used in power system. The proportional term in the controller produces an output that is proportional to the present error value. The response can be adjusted by multiplying the error with a constant which is called the proportional gain constant K_P. The value of K_P should be neither too high nor too low else the control action will be too small and the system may become unstable respectively. The integral term corresponds to the accumulated errors from the past. The integral term includes both the magnitude and duration of the error. The proportional integral (PI) controller is a special type of proportional integral derivative controller. In the proposed work the PID controller is used for the robust design of the damping controller for a power system. PID controllers generally provide acceptable control with default tunings. The performance can be improved by properly and carefully tuning the parameters of the controller. The rotor speed deviation signal is taken as the input here. Figure 10 shows the system with a PID controller (Hesham et al., 2021; Panda et al., 2011). In the present work, the PID is tuned by a novel SOA algorithm and these constants found are as under:

$$P = 1.0000 \quad I = 0.2916 \quad D = 1.0000$$

The output of PID is given by

$$\Delta V_{PID} = \left[K_P + \frac{K_I}{s} + K_D s \right] \Delta\omega_m$$

Figure 8 The AHPM with PID controller (see online version for colours)

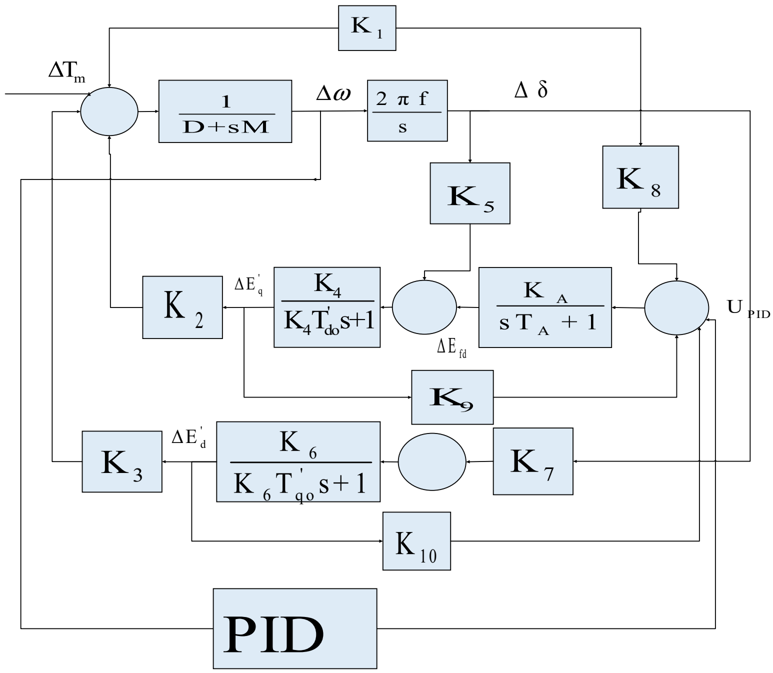

2.9 The ANN technology

The ANN is a branch of artificial intelligence that is based on a biological network of neurons. Neurons are interconnected in various layers of the network. ANN helps in solving real-world problems. It has remarkable computational capabilities and mimics the process of the brain. In the present work, the traditional PID controller is replaced by the ANN controller after feeding the parameters in the custom neural block (Dodangeh and Ghaffarzadeh, 2022). The results of PID and ANN-based SMIBS are compared and shown in various figures. The different activation functions used are tansig, logsig and purelin. The network training function used is trainlm. This function updates the values of weights and biases according to Levenberg-Marquardt optimisation. This algorithm is the fastest backpropagation algorithm, it is the highly recommended first-choice supervised algorithm. The other parameters such as learning rate, epochs, and goals are fed for developing the custom neural network block. Then PID is replaced by that ANN block in the system (Kashki et al., 2010).

3 Problem formulation

3.1 Problem formulation

The time multiplied by absolute error (ITAE) is chosen as the objective function (OF)/ performance index. The parameters of PSS, TCSC and CPT are obtained by SOA. The deviation in rotor speed signal has been chosen as feedback signal for the PSS and TCSC stabilisers. The objective is to minimise the performance index over time (Acharya and Shah, 2018). The OF is $\int_0^{t_{sim}} t\left|\Delta\omega(t)\right| dt.$ The different constraints are given by:

$$K_{PPSSGOA}^{MIN} \le K_{PPSSGOA} \le K_{PPSSGOA}^{MAX}$$
$$T_{1PSSGOA}^{MIN} \le T_{1PSSGOA} \le T_{1PSSGOA}^{MAX} \quad T_{2PSSGOA}^{MIN} \le T_{2PSSGOA} \le T_{2PSSGOA}^{MAX}$$
$$T_{3PSSGOA}^{MIN} \le T_{3PSSGOA} \le T_{3PSSGOA}^{MAX} \quad T_{4PSSGOA}^{MIN} \le T_{4PSSGOA} \le T_{4PSSGOA}^{MAX}$$

$$K_{PPSSMFOA}^{MIN} \le K_{PPSSMFOA} \le K_{PPSSMFOA}^{MAX}$$
$$T_{1PSSMFOA}^{MIN} \le T_{1PSSMFOA} \le T_{1PSSMFOA}^{MAX} \quad T_{2PSSMFOA}^{MIN} \le T_{2PSSMFOA} \le T_{2PSSMFOA}^{MAX}$$
$$T_{3PSSMFOA}^{MIN} \le T_{3PSSMFOA} \le T_{3PSSMFOA}^{MAX} \quad T_{4PSSMFOA}^{MIN} \le T_{4PSSMFOA} \le T_{4PSSMFOA}^{MAX}$$

$$K_{PPSSSOA}^{MIN} \le K_{PPSSSOA} \le K_{PPSSSOA}^{MAX}$$
$$T_{1PSSSOA}^{MIN} \le T_{1PSSSOA} \le T_{1PSSSOA}^{MAX} \quad T_{2PSSSOA}^{MIN} \le T_{2PSSSOA} \le T_{2PSSSOA}^{MAX}$$
$$T_{3PSSSOA}^{MIN} \le T_{3PSSSOA} \le T_{3PSSSOA}^{MAX} \quad T_{4PSSSOA}^{MIN} \le T_{4PSSSOA} \le T_{4PSSSOA}^{MAX}$$

3.2 Different parameters

Table 1 The parameters of GOA, MFOA and SOA

Parameter	*Value*
Population_Size_GOA (N)	20
Maximum Number of Generations_GOA	100
Lower_Bound_KPGOA	1
Upper_Bound_KPGOA	50
Lower_Bound_PSSGOA_T1 to T4	0.01
Upper_Bound_PSS_GOA_T1toT4	1.00
Type of crossover (arithmetic)	2
Dimension_GOA	5
SearchAgents_MFOA	20
Max_Iteration	50
Function_Name_MFOA	F24
Dimension_MFOA	5
Lower_Bound_KPMFOA	1
Upper_Bound_KPMFOA	50
Lower_Bound_PSSMFOA_T1 to T4	0.01
Upper_Bound_PSS_MFOA_T1toT4	1.00
Population_Size_SOA (N)	20
Mxaimum_Number_of_Iterations_SOA (T)	50
Dimesion_SOA (dim)	10
No. of variables for PSS_SOA	5
Upper_Bound_PSS_SOA	1.00

Table 1 The parameters of GOA, MFOA and SOA (continued)

Parameter	*Value*
Lower_Bound_PSS_SOA	0.01
Simulation Time_SOA	10 seconds
T_W for PSS_SOA	10 seconds
T_W for PSS_MFOA	10 seconds
T_W for PSS_SOA	10 seconds

4 Results and analysis

Case a Damping performance comparison with GOA, MFO and SOA algorithms.

4.1 Gain and time constants

Figure 9 shows the simulation diagram of the AHPM with ANN controller. For the models with PSS based on SOA and PID based on SOA the ANN block is replaced by respective controller (Gandhi and Joshi, 2014b).

Table 2 Parameters obtained from three algorithms

S. no.	*GOA*	*MFOA*	*SOA*
K	10	5.7	7.8
T1	0.8	0.7	0.5
T2	0.9	1.0	0.4
T3	0.5	0.2	0.2
T4	0.1	0.5	0.3

4.2 The system A matrix without any PSS or PID

This is the SMIBS state matrix without any device. This is a 5 by 5 matrix due to 5 state variables now instead of earlier 4 by 4 matrix in OHPM.

$$\text{ANODEVICE} = 1.0\text{e}+04 * \begin{bmatrix} 0.0000 & 0.0000 & 0.0000 & 0.0000 & 0.0000 \\ -0.0375 & -0.0000 & 0.0000 & 0.0000 & 1.6000 \\ -0.0051 & 0.0000 & -0.0003 & 0.0000 & 0.0000 \\ -0.0251 & -0.0000 & -0.0001 & 0.0000 & 0.0000 \\ 0.0029 & -0.0000 & 0.0001 & 0.0000 & -0.0040 \end{bmatrix}$$

The A matrix with determined by GOA (including time constants)

$$
1.0e+04 * \begin{bmatrix}
0.0000 & 0.0314 & 0.0000 & 0.0000 & 0.0000 & 0.0000 & 0.0000 & 0.0000 \\
-0.0000 & 0.0000 & -0.0000 & -0.0000 & 0.0000 & 0.0000 & 0.0000 & 0.0000 \\
-0.0000 & 0.0000 & -0.0000 & 0.0000 & 0.0000 & 0.0000 & 0.0000 & 0.0000 \\
-0.0000 & 0.0000 & 0.0000 & -0.0003 & 0.0000 & 0.0000 & 0.0000 & 0.0000 \\
0.1483 & 0.0000 & 0.6969 & 0.3578 & -0.0040 & 0.0000 & 0.0000 & 1.6000 \\
-0.0003 & 0.0000 & -0.0005 & -0.0001 & 0.0000 & -0.0000 & 0.0000 & 0.0000 \\
-0.0003 & 0.0000 & -0.0004 & -0.0001 & 0.0000 & 0.0001 & -0.0001 & 0.0000 \\
-0.0002 & 0.0000 & -0.0005 & -0.0002 & 0.0000 & -0.0000 & 0.0001 & -0.0002
\end{bmatrix}
$$

Figure 9 The AHPM with ANN controller (see online version for colours)

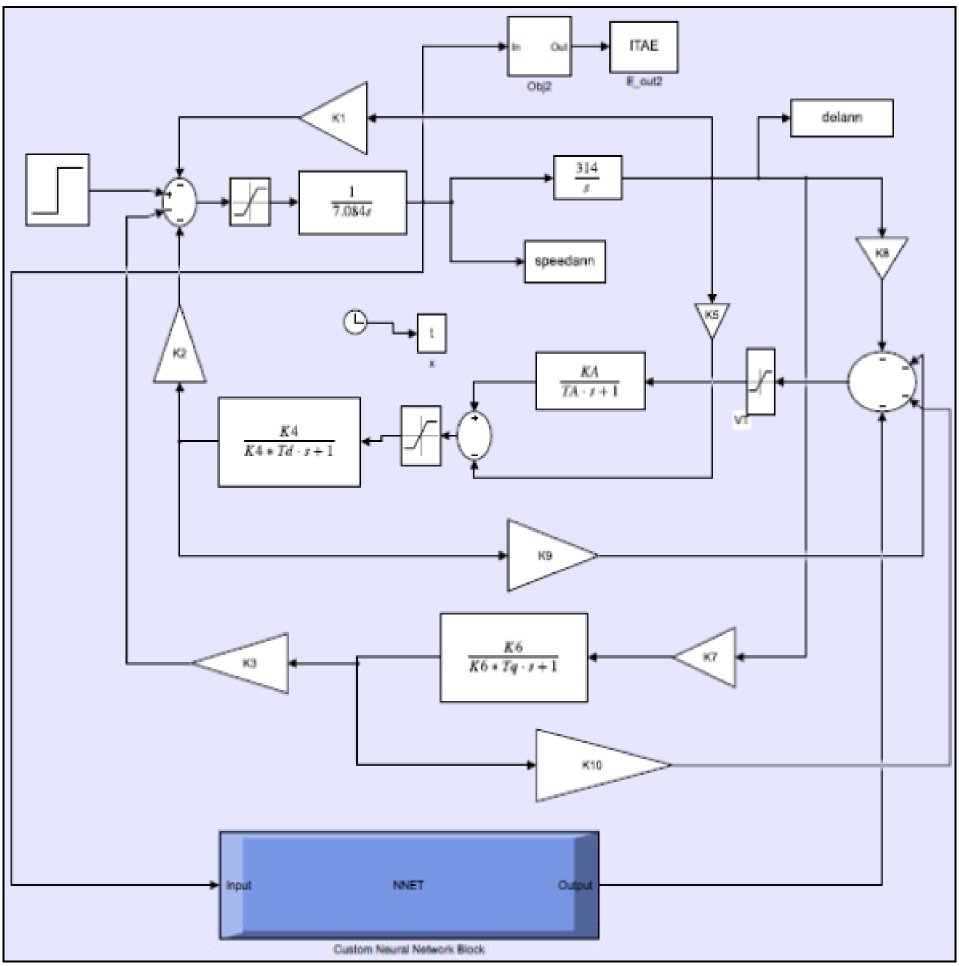

The A matrix with MFO (including time constants)

$$1.0e+04 * \begin{bmatrix} 0 & 0.0314 & 0 & 0 & 0 & 0 & 0 & 0 \\ -0.0000 & 0 & -0.0000 & -0.0000 & 0 & 0 & 0 & 0 \\ -0.0000 & 0 & -0.0000 & 0 & 0.0000 & 0 & 0 & 0 \\ -0.0000 & 0 & 0 & -0.0003 & 0 & 0 & 0 & 0 \\ 0.1483 & 0 & 0.6969 & 0.3578 & -0.0040 & 0.0000 & 0 & 1.6000 \\ -0.0001 & 0 & -0.0001 & -0.0000 & 0 & -0.0000 & 0 & 0 \\ -0.0005 & 0 & -0.0008 & -0.0002 & 0 & 0.0009 & -0.0009 & 0 \\ -0.0001 & 0 & -0.0000 & -0.0000 & 0 & 0.0003 & -0.0002 & -0.0001 \end{bmatrix}$$

The A matrix with SOA (including time constants)

$$1.0e+04 * \begin{bmatrix} 0 & 0 & 0 & 0.0000 & 0 & 0 & 0 & 0 & 0 \\ -0.0375 & -0.0000 & 0 & 0 & 0 & 0 & 0 & 0 & 1.6000 \\ -0.0051 & 0 & -0.0003 & 0 & 0 & 0 & 0 & 0 & 0 \\ -0.0251 & -0.0000 & -0.0001 & 0 & 0 & 0 & 0 & 0 & 0 \\ 0 & 0 & 0 & 0.0002 & -0.0000 & 0 & 0 & 0 & 0 \\ 0 & 0 & 0 & 0.0002 & -0.0000 & -0.0003 & 0 & 0 & 0 \\ 0 & 0 & 0 & 0.0002 & -0.0000 & -0.0001 & -0.0003 & 0 & 0 \\ 0 & 0 & 0 & 0 & 0 & 0 & 0 & 0 & 0 \\ 0.0029 & -0.0000 & 0.0001 & 0.0002 & -0.0000 & -0.0001 & 0.0001 & 0 & -0.0040 \end{bmatrix}$$

The A matrix with PID

$$1.0e+04 * \begin{bmatrix} 0 & 0 & 0 & 0.0000 & 0 & 0 & 0 & 0 \\ -0.0375 & -0.0000 & 0 & 0 & 0 & 0 & 0 & 1.6000 \\ -0.0051 & 0 & -0.0003 & 0 & 0 & 0 & 0 & 0 \\ -0.0251 & -0.0000 & -0.0001 & 0 & 0 & 0 & 0 & 0 \\ 0 & 0 & 0 & 0.0000 & 0 & 0 & 0 & 0 \\ 0 & 0 & 0 & 0.0014 & 0 & -0.0100 & 0 & 0 \\ 0 & 0 & 0 & 0 & 0 & 0 & 0 & 0 \\ 0.0029 & -0.0000 & 0.0001 & 0.0014 & 0.0001 & -0.0100 & 0 & -0.0040 \end{bmatrix}$$

4.3 The participation factor analysis

The participation factor is used to find out the influence of different states on the different modes of the system. The higher the value of elements of participation matrix the higher is the relation between the state variable and corresponding mode. It means the contribution of that state variable is more to that particular eigenvalue or oscillatory mode. For the development of participation matrix right and left eigenvectors are required. The SSS assessment of the system is done using eigenvalue and participation factor analysis of the system. For the stable and secure system, it is essential that all the eigenvalues (EVS) all the modes of the system are stable (Patel and Gandhi, 2018). The participation factor by GOA is

$$\begin{bmatrix} 0.0011 & 0.5274 & 0.4079 & 2.3685 & 0.1088 & 0.0521 & 0.9468 & 156.5874 \\ 0.0002 & 0.0829 & 0.0086 & 0.0106 & 0.0002 & 0.0008 & 0.0127 & 0.0385 \\ 0.0499 & 5.1102 & 0.5318 & 1.0629 & 0.0102 & 0.0545 & 1.6464 & 60.7888 \\ 0.0000 & 0.0056 & 0.0000 & 0.9467 & 0.0000 & 0.0123 & 0.0337 & 0.2987 \\ 2.0681 & 304.2952 & 0.5988 & 4.3572 & 0.0023 & 4.5761 & 9.8009 & 4.1872 \\ 0.0004 & 1.3096 & 0.0026 & 0.0527 & 0.0001 & 0.1196 & 0.1998 & 4.1410 \\ 0.0005 & 2.5869 & 0.0045 & 0.0069 & 0.0003 & 0.4343 & 0.3747 & 3.4045 \\ 0.0000 & 0.3315 & 0.0000 & 0.0000 & 0.0000 & 0.0737 & 0.0002 & 0.0007 \end{bmatrix}$$

The participation factor by MFO is

$$\begin{bmatrix} 0.0013 & 0.2172 & 8.2717 & 4.4629 & 0.0171 & 0.2389 & 1.9133 & 89.6977 \\ 0.0000 & 0.0084 & 0.1673 & 0.0721 & 0.0001 & 0.0097 & 0.0296 & 0.0265 \\ 0.0131 & 1.9930 & 0.0405 & 0.0375 & 0.0002 & 0.1014 & 0.0809 & 3.5704 \\ 0.0000 & 0.0069 & 0.0087 & 0.0081 & 0.0000 & 0.0102 & 1.3376 & 0.9094 \\ 6.5385 & 327.5902 & 5.0344 & 13.3363 & 0.0224 & 30.4995 & 29.7229 & 10.5042 \\ 0.0003 & 0.1483 & 0.0477 & 0.1262 & 0.0001 & 0.0703 & 0.4203 & 43.5615 \\ 0.0000 & 0.0117 & 0.0012 & 0.0865 & 0.0000 & 0.0004 & 0.0050 & 0.5199 \\ 0.0000 & 0.0011 & 0.0000 & 0.0000 & 0.0000 & 0.0164 & 0.0000 & 0.0000 \end{bmatrix}$$

The participation factor by PID based on SOA is

$$\begin{bmatrix} 0.0002 & 0.0000 & 0.0000 & 0.1706 & 0.0007 & 0.2272 & 0 & 0 \\ 99.7002 & 0.5689 & 2.3123 & 32.6896 & 5.4586 & 237.5912 & 0 & 0 \\ 0.0001 & 0.0000 & 0.0001 & 1.9207 & 0.3207 & 49.2543 & 0 & 0 \\ 0.1572 & 0.0001 & 0.0031 & 0.3474 & 0.2144 & 0.1096 & 0 & 0 \\ 0.0002 & 0.0000 & 0.0000 & 0.0085 & 0.0053 & 0.0057 & 0 & 0 \\ 0.0787 & 0.0000 & 0.0049 & 0.0241 & 0.0341 & 0.0087 & 0 & 0 \\ 0 & 0 & 0 & 0 & 0 & 0 & 0 & 0.0000 \\ 0 & 0 & 0 & 0 & 0 & 0 & 0.0000 & 0 \end{bmatrix}$$

The participation factor by PSS based on SOA is

$$\begin{bmatrix} 0 & 0.0000 & 0.0000 & 0.0000 & 0.0000 & 0.0000 & 0.0009 & 0 & 0 \\ 0 & 0.8332 & 8.3212 & 23.0804 & 1.2571 & 2.3054 & 0 & 0 & 0 \\ 0 & 0.0001 & 0.0006 & 0.0968 & 0.0053 & 0.2775 & 0 & 0 & 0 \\ 0 & 0.0016 & 0.0651 & 0.7413 & 0.0317 & 0.0337 & 0 & 0 & 0 \\ 0 & 0.0001 & 0.0044 & 0.1717 & 0.0073 & 0.0260 & 0 & 0 & 0 \\ 0 & 0.0000 & 0.0046 & 0.0121 & 0.0014 & 0.0182 & 0 & 0 & 0 \\ 45.5925 & 0.0000 & 0.0000 & 0.0001 & 0.0002 & 0.0008 & 0 & 0 & 0 \\ 0 & 0 & 0 & 0 & 0 & 0 & 0 & 0 & 0.0255 \\ 0 & 0 & 0 & 0 & 0 & 0 & 0 & 0.0000 & 0 \end{bmatrix}$$

The values of elements in participation matrix by PSS based on SOA are the least. This shows that the contributions of different state variables to the oscillatory modes are least with PSS based on SOA. Hence the best damping is achieved by PSS based on SOA.

4.4 Time domain simulation analysis

Figures 10 to 16 show the results of simulation of models without any controller or no controller (NC), PSS with GOA and PSS with MFOA and PSS with SOA. The variation of rotor angle, rotor speed, field voltage, internal voltage along d-axis and internal voltage along q-axis, power and voltage are shown in various figures. The system response is checked for a 10% step increase in input mechanical power at time t = 1 sec for a loading condition of P = 0.6 pu and Q = 0.0224 pu. From the figures it is observed that the best results are obtained with SOA. The oscillations take less time to settle and overshoot is also less. The system reaches to stable state is a very less time. The control effort is less with SOA. The PSS based on SOA shows the optimum performance. SOA-based PSS is the robust and excellent damping controller.

Figure 10 Rotor angle (case a) (see online version for colours)

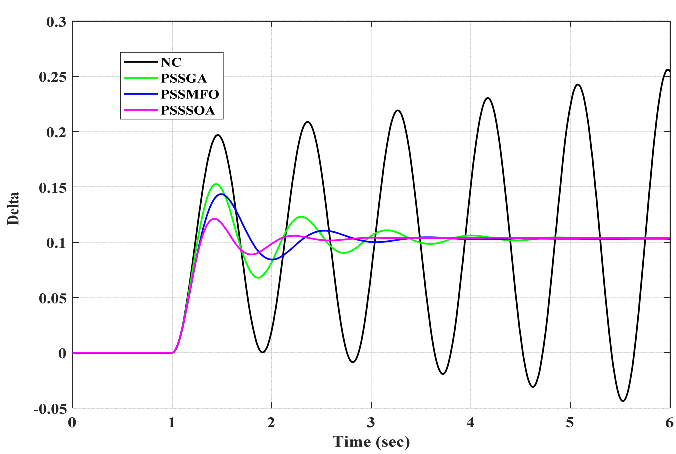

Figure 11 Rotor speed (case a) (see online version for colours)

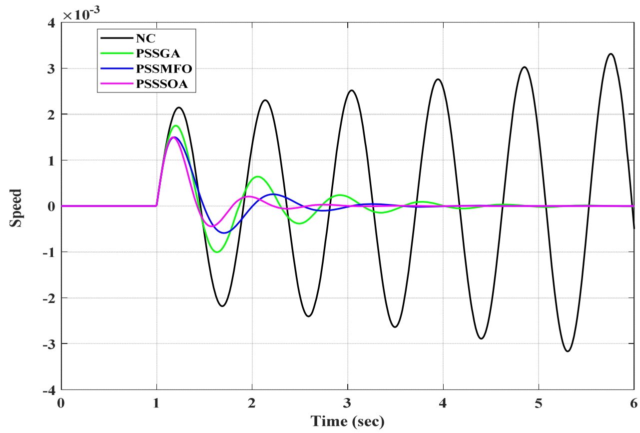

Figure 12 Field voltage (case a) (see online version for colours)

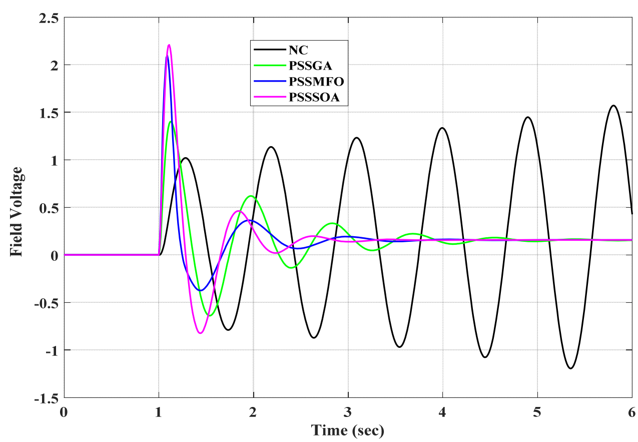

Figure 13 Internal voltage (q-axis) (case a) (see online version for colours)

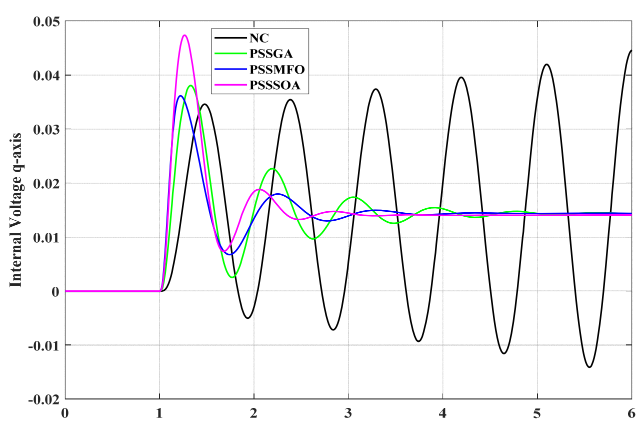

Figure 14 Terminal voltage (case a) (see online version for colours)

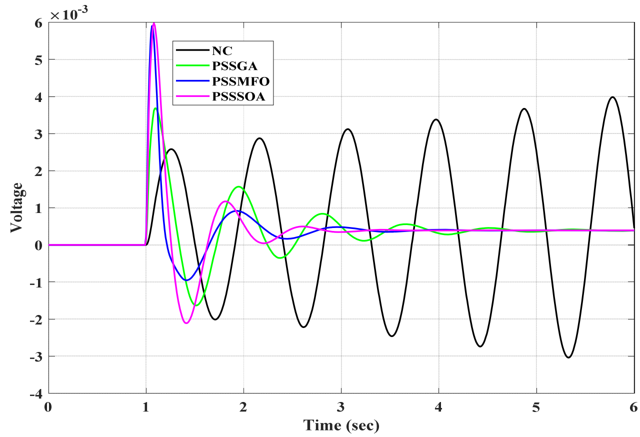

Figure 15 Accelerating power (case a) (see online version for colours)

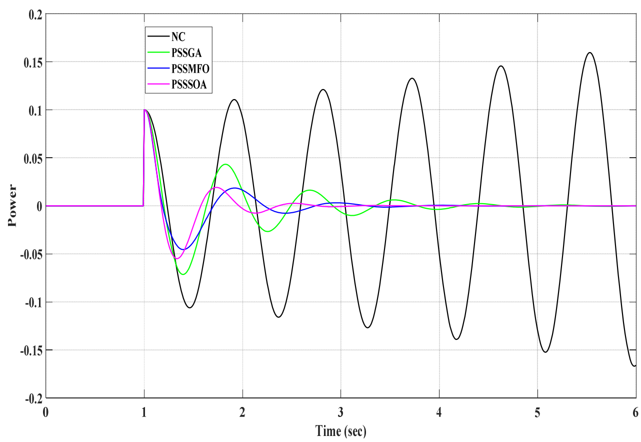

Figure 16 Internal voltage (s-axis) (case a) (see online version for colours)

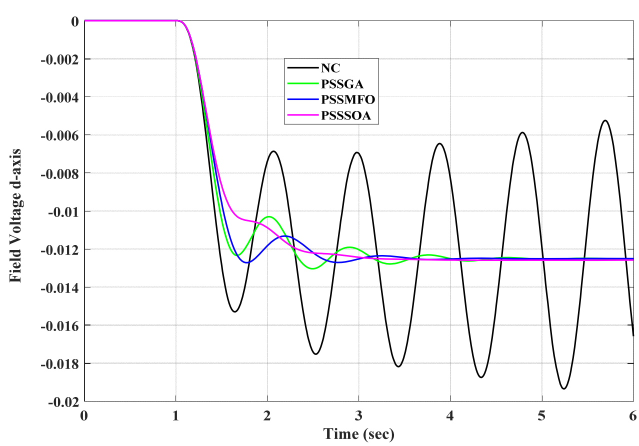

Case b Damping performance comparison between the traditional PID and PSS.

4.5 Time domain simulation analysis with PID and PSS both based on SOA

Figures 17 to 23 show the comparison of the system with NC with the models based on PID and PSS. The various parameters are rotor angle, rotor speed, the internal voltage along the q-axis, the internal voltage along d-axis, field voltage, power, and terminal voltage. From the various figures, it is seen that the results are better with PSS than with PID controller. Both PID and PSS are tuned by SOA. The turning of the PID controller in the presence of disturbances is difficult hence the results are better with PSS based on SOA. The input signal to the PID controller is the speed deviation of the generator. This error is minimised using PID based on SOA.

Figure 17 Rotor angle (case b) (see online version for colours)

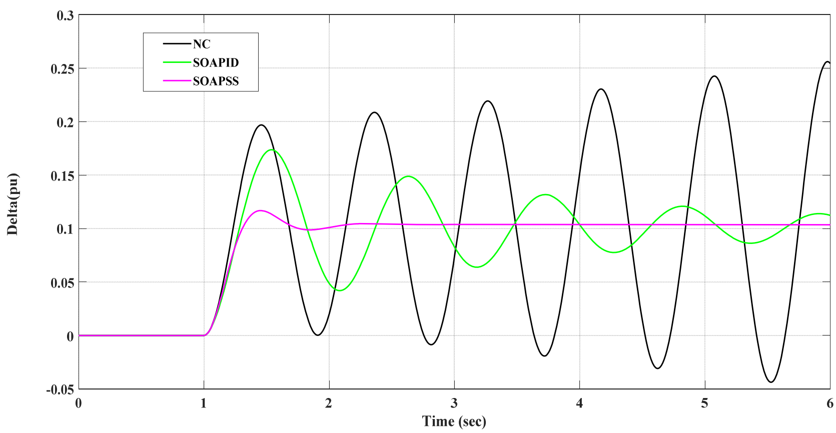

Figure 18 Rotor speed (case b) (see online version for colours)

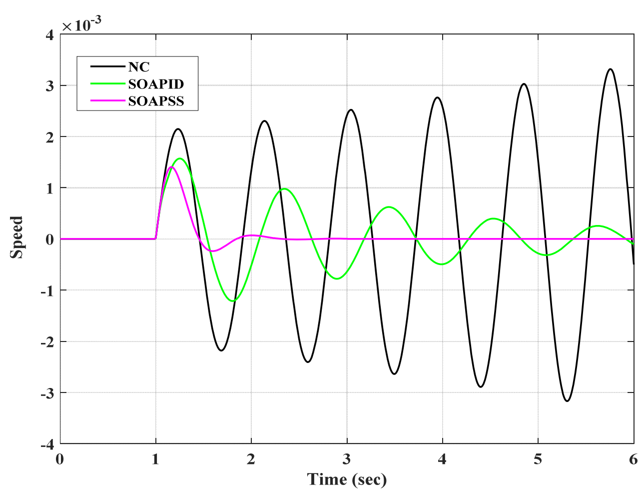

Figure 19 Accelerating power (case b) (see online version for colours)

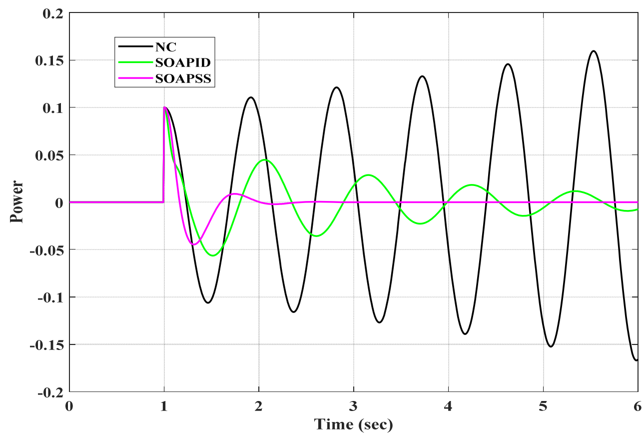

Figure 20 Terminal voltage (case b) (see online version for colours)

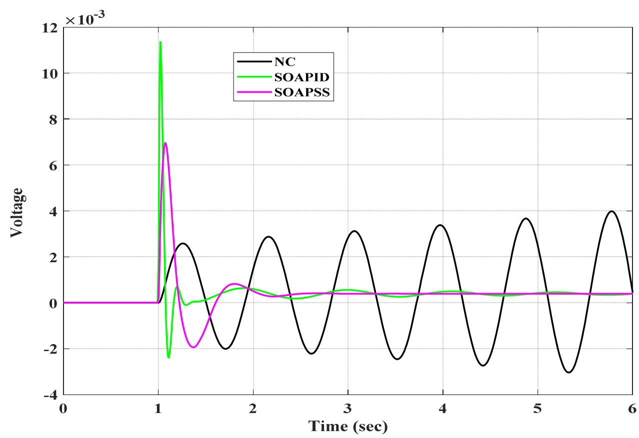

Figure 21 Field voltage (case b) (see online version for colours)

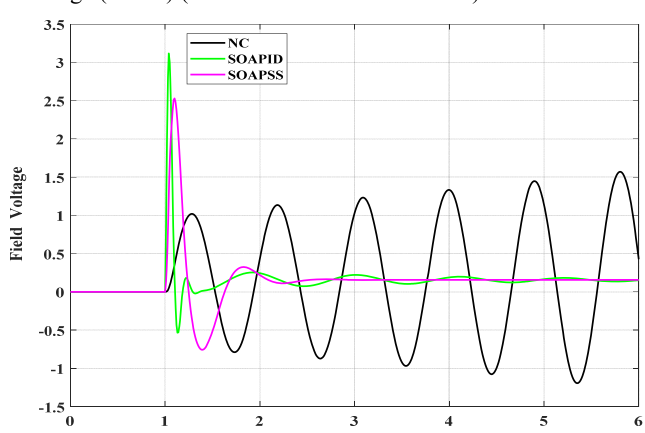

Figure 22 Internal voltage q-axis (case b) (see online version for colours)

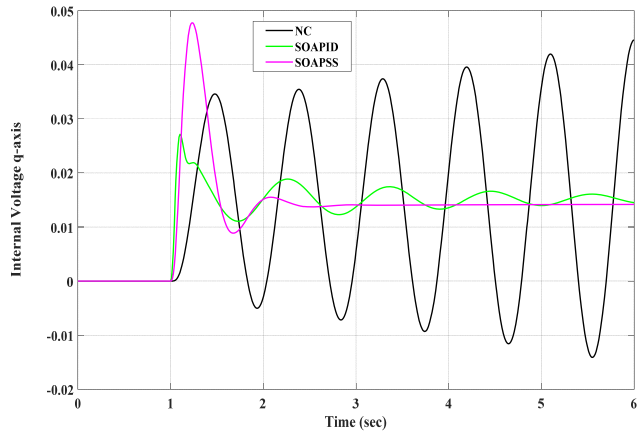

Figure 23 Internal voltage (d-axis) (case b) (see online version for colours)

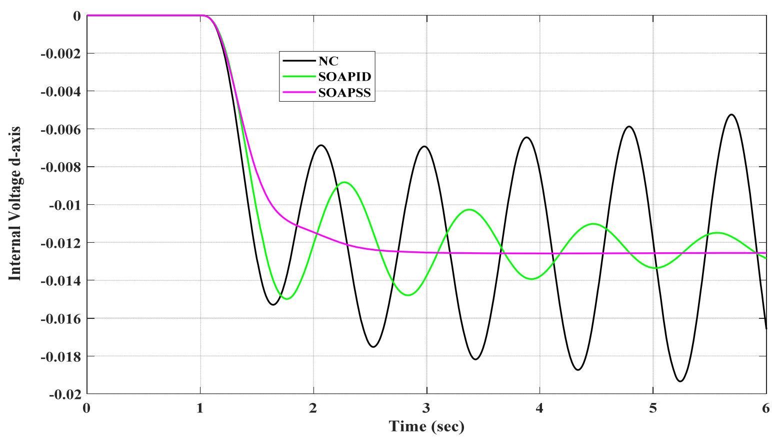

Figure 24 Convergence (see online version for colours)

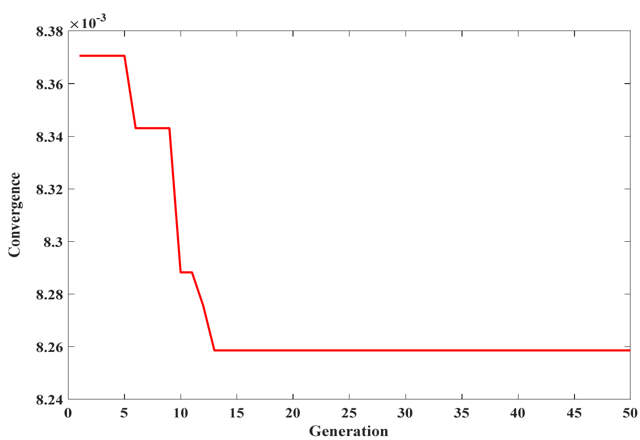

The open loop system is highly unstable. The settling time with PID based on SOA is more than six seconds. The settling time with PSS based on SOA is 2.5 seconds for rotor angle variations.

4.6 Plot of EVS with NC, with GOA, MFOA, SOA and PID

EVS of state matrix A is determined using MATLAB and are known as modes of the system. The damping ratio is calculated from the EVS for stability analysis The EVS may be real or complex. Figures 25 to 29 show the plot of EVS without any controller, with PSS based on GOA, with PSS based on MFOA, with PSS based on SOA, and with PID controller. The real part of the eigenvalue is shown by the X-axis and the Y-axis shows the imaginary part. The real eigenvalue shows the non-oscillatory mode and a negative real eigenvalue shows a decaying mode. The complex eigenvalue occurs in conjugate pairs which corresponds to an oscillatory mode. The real part of the eigenvalue shows the damping and the imaginary part shows the frequency of oscillations (Patel and Gandhi, 2017; Gandotra and Pal, 2022).

Figure 25 EVS with NC (see online version for colours)

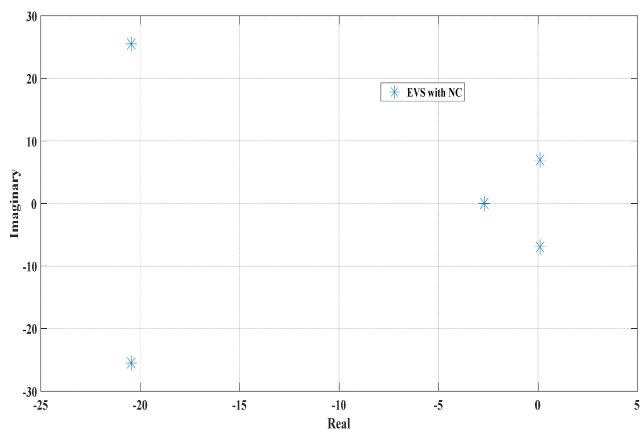

Figure 26 EVS with GOA (see online version for colours)

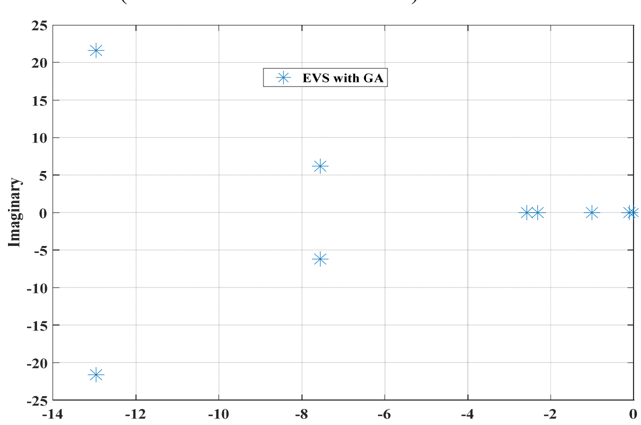

Figure 27 EVS with MOFA (see online version for colours)

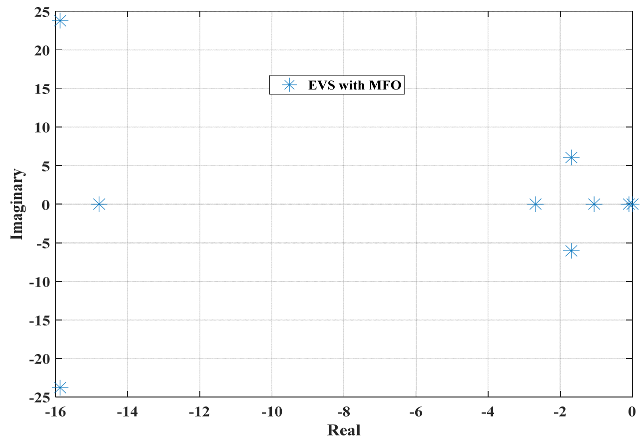

Figure 28 EVS with SOA (see online version for colours)

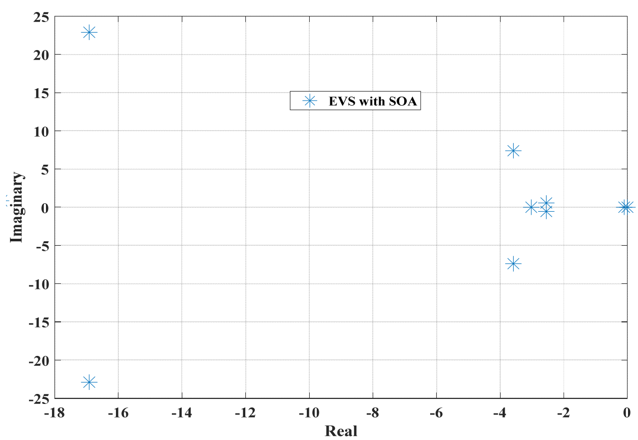

Figure 29 EVS with PID (see online version for colours)

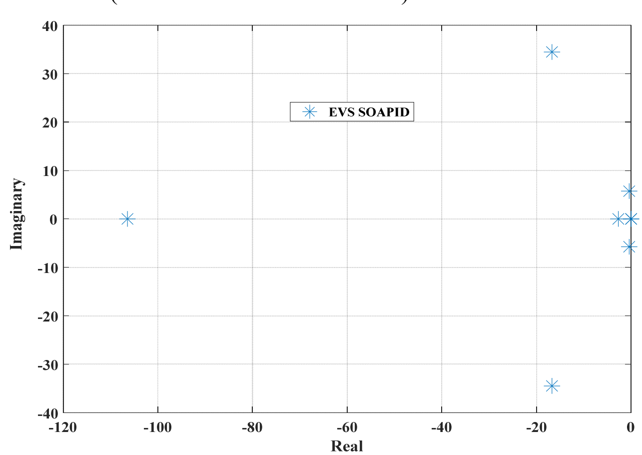

It is required that all the mode, i.e., the EVS should be stable for the robust system. For stability the EVS should lie to the left half of s-plane. From the various figures, the location of EVS with all the models can be compared. The EVS are left to the maximum with SOA-based PSS.

Case c Damping performance comparison between the traditional PID and with ANN.

4.7 Variation in rotor angle and rotor speed

In Figures 30 and 31 shows the variation of rotor angle and speed without any controller and with PID based on SOA (Hashim and Hussien, 2022) and with ANN controller. The open loop system is unstable. The settling times with PID based on SOA are more than six seconds. The settling time with the ANN controller is 2.5 seconds for the rotor angle. The results with ANN controller are similar to PSS based on SOA. Both the PSS based on the optimisation technique SOA and the controller based on artificial intelligence technique which is ANN produced excellent and similar results for damping profile improvement of the system for case studies B and C. This shows that the AHPM with PSS based on SOA and AHPM with ANN controller is both excellent damping controllers as compared to the system with GOA, MFOA, or PID controllers.

Figure 30 Rotor angle (case c) (see online version for colours)

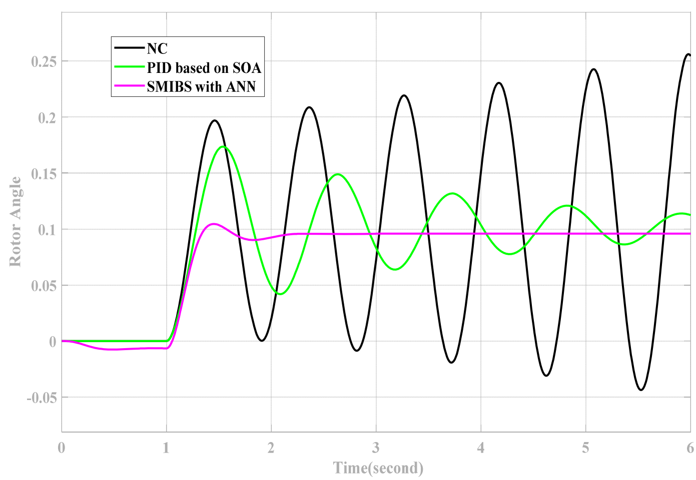

This shows that optimisation algorithm-based controller and the artificial intelligence technology-based ANN controller is excellent for damping control. The participation matrix showed the relation or the degree of association between the EVS and the rotor modes of the system. The value of elements of the participation matrix with SOA-based PSS is less. Overall, the system is found to be robust with SOA-based AHPM. The system performance with PID based on SOA is compared with PSS based on SOA and with ANN controller. For case studies B and C, the controllers PSS with SOA and ANN controller is found to be producing similar results.

Figure 31 Rotor speed (case c) (see online version for colours)

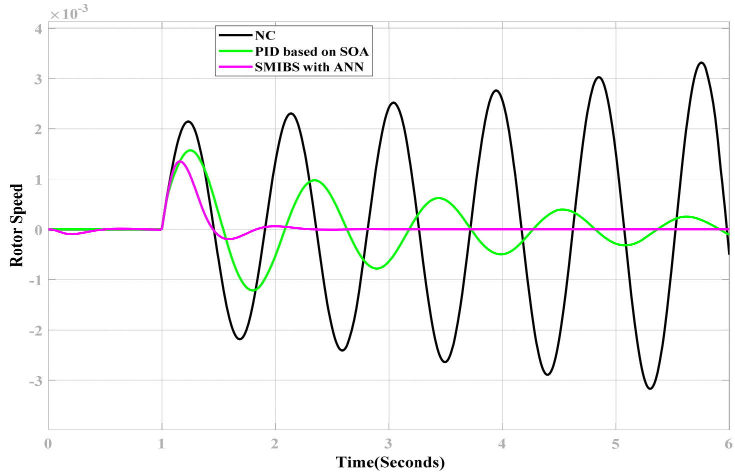

5 Conclusions

In the present paper, a novel AHPM is developed for designing the power system. This model has five state variables instead of the four state variables used in the old HP model. The study is performed on the detailed model of SG without neglecting the dynamics of the d-axis internal voltage. The parameters are optimised by a novel SOA which has excellent exploration and exploitation features. Robust power system is developed with AHPM based on SOA and this is observed from the variation in various parameters shown in various figures. The system EVS are shifted to the more left half of the s-plane which indicates an improvement in stability. The damping ratios are higher with PSS based on SOA model. The higher the damping ratio, the more is the stability of the system. The oscillations are settled faster and system stability is improved with PSS controller based on SOA and AHPM. It is suggested that both controllers (based on optimisation technique SOA and ANN methodology) are excellent as compared to systems based on GOA, MFOA, and PID controllers. The AHPM model is capable of meeting the challenges of grid integration with renewables. There will be no interruption in power supply and hence no obstacle in the growth and development of country.

References

Acharya, A.G. and Shah, B.J. (2018) 'Small signal stability improvement of multimachine power system using power system stabilizer', *International Journal of Electrical Engineering and Technology*, Vol. 9, No. 2, pp.62–74.

Anantwar, H., Sundar, S. and Lakshmikantha, B.R. (2019) 'Optimal controllers design for voltage control in off-grid hybrid power system', *International Journal of Electrical and Computer Engineering*, December, Vol. 9, No. 6, pp.4586–4597.

Das, G., Panda, R., Samantaray, L. and Agrawal, S. (2022) 'A novel non-entropic objective function for multilevel optimal threshold selection using adaptive equilibrium optimizer', *Iranian Journal of Electrical and Electronic Engineering*, Vol. 2, No. 2, pp.1–10.

Dodangeh, M. and Ghaffarzadeh, N. (2022) 'An intelligent machine learning-based protection of AC microgrids using dynamic mode decomposition', *Iranian Journal of Electrical and Electronic Engineering*, Vol. 4, No. 2544, pp.1–9.

Gandhi, P.R. and Joshi, S.K. (2013) 'GA and ANFIS based power system stabilizer', *IEEE*, pp.1–7 [online] https://ieeexplore.ieee.org/document/6672689.

Gandhi, P.R. and Joshi, S.K. (2014a) 'Smart control techniques for design of TCSC and PSS for stability enhancement of dynamical power system', *Applied Soft Computing*, Vol. 24, pp.664–668, Elsevier, https://doi.org/10.1016/j.asoc.2014.08.017.

Gandhi, P.R. and Joshi, S.K. (2014b) 'Design of power system stabilizer using genetics algorithm based neural network', *Journal of Electrical Engineering*, Vol. 14, No. 2, pp.1–13.

Gandhi, P.R. and Joshi, S.K. (2019) 'Soft computing techniques for designing of adaptive power system stabilizer', *IEEE*, pp.1–4 [online] https://ieeexplore.ieee.org/document/8810851.

Gandotra, R. and Pal, K. (2022) 'FACTS technology: a comprehensive review on FACTS optimal placement and application in power system', *Iranian Journal of Electrical and Electronic Engineering*, Vol. 18, No. 3, pp.1–14.

Hashim, F.A. and Hussien, A.G. (2022) 'Snake optimizer: a novel meta-heuristic optimization algorithm', *Knowledge-Based Systems*, Vol. 242, pp.1–34, Elsevier.

Hesham, A., El-Kareem, A., Elhameed, M.A. and Elkholy, M.M. (2021) 'Effective damping of local low frequency oscillations in power systems integrated with bulk PV generation', *Protection and Control of Modern Power Systems*, pp.1–16, https://doi.org/10.1016/j.knosys.2022.108320.

Jyothi, R., Holla, T., Rao, K.U. and Jayapal, R. (2021) 'Machine learning based multi class fault diagnosis tool for voltage source inverter driven induction motor', *International Journal of Power Electronics and Drive Systems*, June,, Vol. 12, No. 2, pp.1205–1215.

Kashki, M., Abdel-Magid, Y.L. and Abido, M.A. (2010) 'Pole-placement approach for robust optimum design of PSS and TCSC-based stabilizers using reinforcement learning automata', *Electrical Engineering*, Vol. 91, pp.383–394, Springer [online] https://link.springer.com/article/10.1007/s00202-010-0147-5#citeas.

Mahapatra, S., Malik, N. and Jha, A.N. (2019) 'Cuckoo search algorithm and ant lion optimizer for optimal allocation of TCSC and voltage stability constrained optimal power flow', *International Conference on Intelligent Computing and Smart Communication, Algorithms for Intelligent Systems*, Springer Nature Singapore Pte, Ltd., pp.889–905.

Mahapatra, S., Raj, S. and Krishna, S.M. (2020) 'Optimal TCSC location for reactive power optimization using oppositional SALP swarm algorithm', *Innovation in Electrical Power Engineering, Communication, and Computing Technology, Lecture Notes in Electrical Engineering*, Springer Nature Singapore Pte Ltd., pp.413–424.

Mallikarjunaswamy, S., Sharmila, N., Maheshkumar, D., Komala, M. and Mahendra, H.N. (2020) 'Implementation of an effective hybrid model for islanded microgrid energy management', *Indian Journal of Science and Technology*, Vol. 20, No. 13, pp.2733–2746.

Nie, Y., Zhang, Y., Zhao, Y., Fang, B. and Zhang, L. (2019) 'Wide-area optimal damping control for power systems based on the ITAE criterion', *International Journal of Electrical Power & Energy Systems*, March, Vol. 106, No. 4, pp.192–200.

Padhy, S. and Panda, S. (2021) 'Application of a simplified grey wolf optimization technique for adaptive fuzzy PID controller design for frequency regulation of a distributed power generation system', *Protection and Control of Modern Power Systems*, Vol. 6, No. 2, pp.1–16 [online] https://pcmp.springeropen.com/articles/10.1186/s41601-021-00180-4.

Padiyar, K.R. (2008) *Power System Dynamics Stability and Control*, BS Publications, 2nd ed., BS Publications, Hyderabad.

Panda, S. (2009) 'Differential evolution algorithm for TCSC-based controller design', *Simulation Modelling Practice and Theory*, Vol. 17, No. 10, pp.1618–1634, [online] https://www.sciencedirect.com/science/article/abs/pii/S1569190X09000987.

Panda, S., Swain, S.C., Baliarsingh, A.K. and Ardil, C. (2011) 'Optimal supplementary damping controller design for TCSC employing RCGA', *World Academy of Science, Engineering and Technology, International Journal of Electrical and Computer Engineering*, Vol. 5, No. 11, pp.1600–1609.

Patel, A. and Gandhi, P.R. (2017) 'Damping oscillations in detail model of synchronous generator using PSO based PSS', *IEEE*, pp.1–6 [online] https://ieeexplore.ieee.org/document/7853470.

Patel, A. and Gandhi, P.R. (2018) 'Damping low frequency oscillations using PSO based supplementary controller and TCSC', *International Conference on Power Energy, Environment and Intelligent Control*, IEEE, pp.38–43.

Sahu, P.R., Hota, P.K., Panda, S., Lenka, R.K., Padmanaban, S. and Blaabjerg, F. (2021) 'Coordinated design of FACTS controller with PSS for stability enhancement using a novel hybrid whale optimization algorithm – Nelder Mead approach', *Electric Power Components and Systems*, Vol. 49, Nos. 16–17, pp.1–28, Taylor and Francis Online.